Defence Technology 17 (2021) 202–211

Contents lists available at ScienceDirect

Defence Technology

journal homepage: www.keaipublishing.com/en/journals/defence-technology

Damage modeling of ballistic penetration and impact behavior of concrete panel under low and high velocities

Chahmi Oucif [a, *], J.S. Kalyana Rama [b, c], K. Shankar Ram [b, d], Farid Abed [e]

[a] Institute of Structural Mechanics (ISM), Bauhaus-Universität Weimar, Marienstraße 15, D-99423, Weimar, Germany
[b] Department of Civil Engineering, BITS Pilani-Hyderabad Campus, Hyderabad, 500072, India
[c] Department of Civil Engineering, Vignana Bharathi Institute of Technology, Hyderabad, 501301, India
[d] Department of Civil Engineering, University of California, Berkeley, Berkeley, CA, United States
[e] Department of Civil Engineering, American University of Sharjah, P.O. Box 26666, United Arab Emirates

ARTICLE INFO

Article history:
Received 30 December 2019
Received in revised form
8 March 2020
Accepted 23 March 2020
Available online 31 March 2020

Keywords:
Johnson-Holmquist-2
Concrete damage plasticity
Concrete panel
Damage
Impact loads

ABSTRACT

This work presents a numerical simulation of ballistic penetration and high velocity impact behavior of plain and reinforced concrete panels. This paper is divided into two parts. The first part consists of numerical modeling of reinforced concrete panel penetrated with a spherical projectile using concrete damage plasticity (CDP) model, while the second part focuses on the comparison of CDP model and Johnson-Holmquist-2 (JH-2) damage model and their ability to describe the behavior of concrete panel under impact loads. The first and second concrete panels have dimensions of 1500 mm × 1500 mm × 150 mm and 675 mm × 675 mm × 200 mm, respectively, and are meshed using 8-node hexahedron solid elements. The impact object used in the first part is a spherical projectile of 150 mm diameter, while in the second part steel projectile of a length of 152 mm is modeled as rigid element. Failure and scabbing characteristics are studied in the first part. In the second part, the comparison results are presented as damage contours, kinetic energy of projectile and internal energy of the concrete. The results revealed a severe fracture of the panel and high kinetic energy of the projectile using CDP model comparing to the JH-2 model. In addition, the internal energy of concrete using CDP model was found to be less comparing to the JH-2 model.

1. Introduction

Concrete is the most advantageous material used in the construction of structures due to its resistance of the effect of blast [1]. It becomes ductile when is appropriately reinforced, especially under tensile loads [2–4], and is transformed into the most suitable material in the construction of nuclear and protective infrastructures due to the improvement in its strength and performance. The study of impact behavior of reinforced concrete structures has received much attention over the last decades [5,6] [4,7–20]. The analysis of damage in materials has also received much attention [21–25].

Many experimental studies have been conducted on the description of the impact behavior of reinforced concrete (RC) structures, in which the results showed that the RC structures exhibit high resistance when high concrete strength is used [26]. In (Dechun et al., 2017). It was exceptionally revealed that the increase in the compressive strength influences minorly the impact resistance of the RC concrete slab. Borvik et al. [27] studied experimentally the ballistic penetration of steel fiber reinforced high-performance concrete slabs penetrated by steel projectiles. A low increase of 20% in the ballistic limit velocity was obtained when the unconfined compressive strength of the concrete increases. Levi-Hevroni et al. [26] studied the behavior of shaped concrete samples under dynamic tension. [47] studied the plasticity model and a damage-plasticity model of a 3D concrete specimen with the help of finite element analysis. They observed and studied the variation between the predicted and actual material behavior. Aslani and Nejad [28] developed three new models for the fracture study on SCC and conventional concrete both. These models included elastic

* Corresponding author.
E-mail addresses: chahmi.oucif@uni-weimar.de, chahmi.oucif@uni-weimar.de (C. Oucif), kalyan@vbithyd.ac.in (J.S. Kalyana Rama), connect.shankar31@gmail.com (K. Shankar Ram), fabed@aus.edu (F. Abed).
Peer review under responsibility of China Ordnance Society

https://doi.org/10.1016/j.dt.2020.03.013

model, tensile strength model and a compressive stress-strain model. These models were also verified against the experimental results. Grégoire et al. [29] compared experimental results with numerical simulations performed with reference to an integral non local model. Francisco Lopez-Almansa et al. [30] in their work have strained on the significance of concrete damage plasticity (CDP) model being able to reproduce the actual geometric non-linear behavior of concrete RC frames as compared to other computational models like distributed plasticity models or lumped plasticity models. Temsah et al. [31] fundamentally focused on the feasibility of using a finite element software to simulate blast loading on reinforced concrete beams using CDP model. The blast load is numerically designed using the built in CONWEP model in ABAQUS with an acceptable margin of error. Numerous studies were made on the effect of impact loading on different types of structural elements. Othman and Marzouk0 [32] used a constitutive CDP model to analyse the behavior of concrete under different rates of impact loading. Liu et al.[33] studied the impact responses of plain concrete and ultra high-performance concrete (UHPC) under high-velocity impact conditions. The numerical model resulted in inaccurate crater diameter results but had captured the depth of penetration of UHPC targets. Drathi et al. [34] used stochastic simulations based on the element-free Galerkin method to predict upper and lower bounds of the impact resistance of concrete structures. Kalyana Rama J. S., et al. [35] developed input parameters for CDP model based on the stress-strain models of concrete to evaluate the fracture properties of concrete. The proposed model was in good agreement with experimental values of size independent fracture energy. Kota S K., et al. [36] had successfully simulated the response of RC frames subjected to seismic loads using CDP model. The input parameters for the study were obtained from existing stress-strain models of concrete. Columns, beams and beam-column joints were strengthened using varying thickness of UHPFRC strips. It was concluded that the CDP model can be used to predict the behaviour of RC frames subjected to gravity and lateral loads.

The present work aims at analysing the impact behavior of plain and reinforced concrete panels under impact loads. CDP model is used to simulate the impact behavior of reinforced concrete panel penetrated with a spherical projectile. Few studies have been conducted in literature on the comparison of CDP and Johnson-Holmquist-2 (JH-2) damage models. In the present paper, comparison of impact behavior and kinetic and internal energies in plain concrete panel is investigated.

2. Concrete damage plasticity (CDP) model

The Druker-Prager strength hypothesis is often used for determining the failure behavior of concrete. The failure, according to the hypothesis, is determined by the non-dilatational strain energy (the difference between total strain energy and the strain energy resulting from volume change) and the boundary surface itself, in the stress space, assumes the shape of a cone. The advantages of this theory are the surface smoothness and no complications in computing. But, the theory is inconsistent with the actual behavior of concrete.

The CDP model is modified from the Druker-Prager strength hypothesis. In CDP model the failure cross-section in the deviatoric plane need not to be a circle (as in Druker-Prager hypothesis) but can be any shape, which is determined by the parameter K_c (Lubnineret et al., 1989). K_c is interpreted as the ratio of distances between hydrostatic axis and compression and tension meridians, respectively, in the deviatoric cross-section. $K_c = 1$ implies it's a circle. [43] recommends value of 2/3. $(\sigma_{b0}/\sigma_{c0})(f_{b0}/f_{c0})$ is defined as the ratio of compressive strength in bi-axial state to that in uniaxial state. The value comes out to 1.16248. [43] recommends the value of σ_{b0}/σ_{c0} as 1.16.

Dilation angle, ψ, is the angle of inclination of the failure surface towards the hydrostatic axis, measured in the meridional plane. Physically, it can be understood as the angle of internal friction of concrete. It generally takes values between 36° and 40°. In CDP, the plastic potential surface takes the shape of a hyperbola. The shape of the hyperbola can be adjusted through the parameter eccentricity. It is small positive value which expresses the rate of approach of the hyperbola to its asymptote. Eccentricity Parameter can be calculated as the ratio of tensile strength to compressive strength [37]. The CDP model recommends the value of eccentricity, ε, as 0.1. When, $\varepsilon = 0$, the meridional plane becomes a straight line as in classic Druker-Prager hypothesis.

The viscosity parameter slightly helps in reduction in the step size, in order to regularize the constitutive equations. Viscoplastic adjustment consists in choosing viscosity parameter, μ, to be greater than zero such that the ratio of problem's time step to μ tends to infinity. Hence, value of viscosity parameter for viscoelastic materials should be as small as possible. For non-viscoelastic materials, the value is recommended to be 0 [38].

These five factors, namely $K_c\sigma_{b0}/\sigma_{c0}$, ψ, ε and μ, along with the stress-strain behaviors in compression and tension and variation of damage with inelastic strain (in compression) and with cracking strain (in tension) are the input parameters for the CDP model, in Abaqus/CAE.A summary of the above is tabulated in Table 1.

Concrete damaged plasticity is capable of modeling all structural types of reinforced or unreinforced concrete or other quasi-brittle materials subjected to monotonic, cyclic or dynamic loads. This model is based on a coupled damage plasticity theory and the multi-axial behavior of concrete in damaged plasticity model governs by a yield surface which is proposed by Lubliner et al. [39] and was modified later by Refs. [40]. Tensile cracking and compressive crushing of concrete are two assumed main failure mechanisms in this model. Furthermore, the degradation of material for both tension and compression behaviors have been considered in this model. The concrete damage plasticity parameter for the ultra-high strength concrete is found out based on the idealized bilinear stress-strain response tested using experimental investigation on dog-bone specimen. Fig. 1, Fig. 2 and Fig. 3 represent the constitutive relation of the material used to simulate the numerical behavior of the structural response.

The schematic diagrams represents the stress-strain behavior of plain concrete in uniaxial compression amd tensile behavior of the normal strength concrete respectively.

where.

E_0 = Modulus of elasticity (N/mm^2) σ_{c0} = Cracking compressive stress (N/mm^2);
σ_{cu} = Ultimate compressive stress (N/mm^2) d_c = Compression damage parameter
ε_c^{pl} = Plastic strain ε_c^{el} = elastic strain
σ_t = Tensile stress (N/mm^2); σ_{t0} = Cracking tensile stress (N/mm^2);

Table 1
Summary of CDP parameters.

Parameter	Recommended Value
K_c	23
$\sigma_{b0}\sigma_{c0}$	1.16
Dilation Angle, $\psi_{/(^\circ)}$	38
Eccentricity, ε	0.1
Viscosity Parameter, μ	0

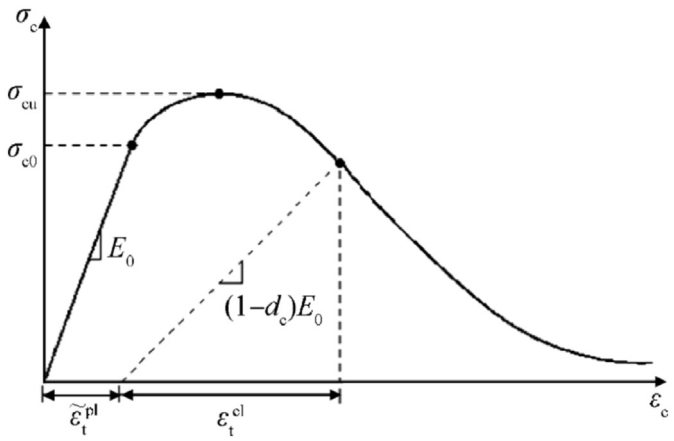

Fig. 1. Response of normal strength concrete to uniaxial compression loading.

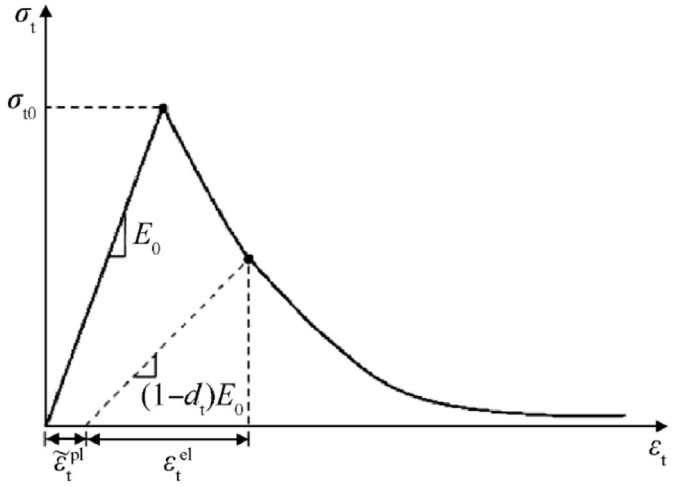

Fig. 2. Response of normal strength concrete to uniaxial tension loading.

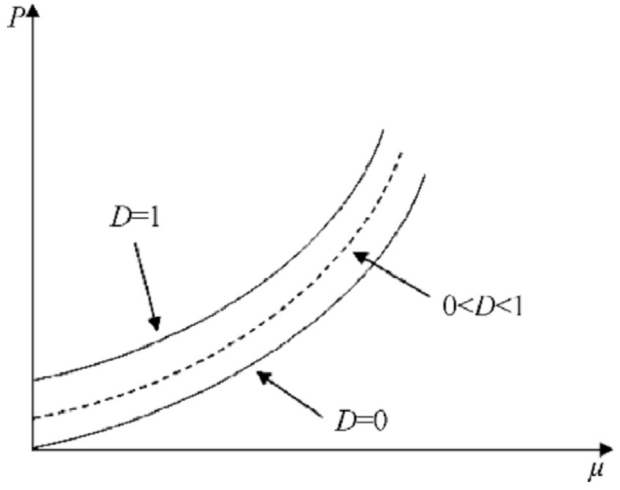

Fig. 3. Pressure-volumetric strain relationship of the JH-2 model.

ε_{ck} = cracking strain ε_t^{pl} = Plastic strain (tensile behavior)
ε_t^{el} = elastic strain (tensile behavior) d_t = Tensile damage parameter

σt = Tensile stress (N/mm^2); σt0 = Cracking tensile stress (N/mm^2);
ε_{tc} = cracking strain ε_u = ultimate tensile strain

3. Johnson-Holmquist damage model (JH-2)

Several constitutive models have been used in literature for the description of the dynamic behavior of brittle materials under impact loads. In this paper, the Johnson-Holmquist damage (JH-2) model is used to analyse the impact behavior of reinforced concrete panel penetrated by a ogive-nosed steel projectile. The JH-2 is the second version of the Johnson-Holmquist (JH-1) ceramic model [41] that is able to simulate the impact behavior of brittle materials such dilatation, pressure-strength dependence, strain-rate effect resulted by damage [48]. According to the JH-2 model, the yield strength degrades with damage accumulation whereas in the JH-1 model the yield strength degrades when critical damage is reached. The strength is defined in terms of the equivalent stress as follows:

$$\sigma^* = \sigma_i^* - D\left(\sigma_i^* - \sigma_f^*\right) \tag{1}$$

Where, σ_i^* is the normalized intact equivalent stress, D is the damage variable, and σ_f^* is the normalized fractured equivalent stress. It should be noted that the intact and fully damaged materials are represented by the damage values $D = 0$ and $D = 1$, respectively. The equations of the strength can also be defined in a general form by normalizing the terms in Eq. (1) to the equivalent stress at the Hugoniot elastic limit (HEL), which corresponds to one-dimensional shock wave that exceeds the elastic limit as follows:

$$\sigma_{HEL} = \frac{3}{2}(HEL - P_{HEL}) \tag{2}$$

where P_{HEL} is the pressure at the Hugoniot Elastic Limit. After normalization, Eq. (1) of the strength can be rewritten as

$$\sigma^* = \frac{\sigma}{\sigma_{HEL}} \tag{3}$$

According to the JH-2 model, it is assumed that the equation of the strength in the case of the undamaged and fully damaged material states can be, respectively, expressed as function of pressure and strain rate as follows:

$$\sigma_i^* = A(P^* + T^*)^N(1 + C\ln\varepsilon^*) \le \sigma_i^{max} \tag{4}$$

$$\sigma_f^* = B(P^*)^M(1 + C\ln\varepsilon^*) \le \sigma_f^{max} \tag{5}$$

where the material parameters are A, B, C, M, and N, and strengths limits σ_i^{max} and σ_f^{max}. The normalized pressure is defined as

$$P^* = \frac{P}{P_{HEL}} \tag{6}$$

where P is the actual pressure. The normalized maximum tensile hydrostatic pressure is also written as

$$T^* = \frac{T}{T_{HEL}} \tag{7}$$

where T is the maximum tensile pressure supported by the material. The strain rate is given by $\dot{\varepsilon}^{pl} = \dot{\bar{\varepsilon}}^{pl}/\dot{\varepsilon}_0$, where $\dot{\bar{\varepsilon}}^{pl}$ is the equivalent plastic strain rate. The JH-2 model uses similar damage

accumulation of the Johnson-Cook model and assumes that damage increases along with the plastic strain as follows:

$$D = \sum \frac{\Delta\bar{\varepsilon}^{pl}}{\bar{\varepsilon}_f^{pl}(P)} \tag{8}$$

where

$$\bar{\varepsilon}^{pl} = D_1(P^* + T^*)^{D_2};\ \bar{\varepsilon}_{f,min}^{pl} \le \bar{\varepsilon}^{pl} \le \bar{\varepsilon}_{f,max}^{pl} \tag{9}$$

It should be noted that $\Delta\bar{\varepsilon}^{pl}$ is the increment of the equivalent plastic strain, and $\bar{\varepsilon}_f^{pl}(P)$ is the equivalent plastic strain at failure. D_1 and D_2 are material constants. The parameters $\bar{\varepsilon}_{f,min}^{pl}$ and $\bar{\varepsilon}_{f,max}^{pl}$ are introduced for the limitation of minimum and maximum values of the fracture strain. The pressure-volume relationship of the brittle materials is defined as

$$P = \begin{cases} K_1\mu + K_2\mu^2 + K_3\mu^3 & if\ \mu \ge 0\ (\text{compression}) \\ K_1\mu & if\ \mu < 0\ (\text{tension}) \end{cases} \tag{10}$$

where K_1, K_2, K_3 are material constants, and $\mu = \rho/\rho_0 - 1$ with ρ and ρ_0 the current and reference densities, respectively. When the material fails, an additional pressure increment ΔP is included which takes the following expression:

$$P = K_1\mu + K_2\mu^2 + K_3\mu^3 + \Delta P \tag{11}$$

The determination of the pressure increment is determined based on the energy consideration. When the material is damaged, the deviatoric elastic energy ΔU decreases due to the decrease on strength. Fig. 3 shows the relationship pressure-volumetric strain according to the JH-2 model.

The decrease of the elastic energy is converted into the potential energy by the increase of the pressure increment ΔP, such that

$$\Delta P_{t+\Delta t} = -K_1\mu_{t+\Delta t} + \sqrt{(K_1\mu_{t+\Delta t} + \Delta P_t)^2 + 2\beta K_1 \Delta U} \tag{12}$$

where β is the fraction of the elastic energy increase converted to potential energy ($0 \le \beta \le 1$).

4. Numerical modeling

4.1. RC panel penetrated with spherical projectile

A 150 mm thick RC slab panel of dimensions 1500 mm × 1500 mm is modeled to assess its impact resistance to a spherical projectile under low velocity. Uniform reinforcement of 8 mm diameter bars with equal spacing are provided in both the directions of the slab as shown in Fig. 4. The lengths of the bars adopted for both directions are set to unequal/different values to ensure a positive protrusion at the edges where they meet. This is done to avoid perfect coincidence of the tips of the bars, as that would lead to a zero-truss length error, which was one of the initial difficulties faced while modeling the slab. The diameter of the spherical projectile is chosen to be 150 mm for the present study. Mesh sensitivity analysis was performed to ensure that the accuracy of the model was maintained throughout the analysis. Various combinations of mesh sizes varying from 150 mm to 60 mm with an interval of 10 mm are chosen for the convergence study. In order to obtain a relatively finer-medium sized mesh, different seed sizes of 60 mm, 30 mm and 15 mm are given for the slab in such a way that it becomes increasingly finer towards the point of impact. Benchmarking of final mesh size was done based on the von mises stresses obtained. The slab is designated as an independent part (in assembly) the rest of the instances are designated as dependent instances (to be meshed part by part). Explicit (3D stress) C3D8R (Cube three-dimensional eight node reduced integration) Hex-dominated elements with 8-node linear brick, reduced integration, hourglass control is used in the meshing and the number of elements present in the slab are 12500. Stirrups and longitudinal bars are tied using tie constraint and embedded constraint is used to embed steel into concrete.Reinforcing Steel rebars are modeled as three dimensional truss element (T3D2). A 2-node straight truss element, which uses linear interpolation for position and displacement, has a constant stress. It is defined that the cross-sectional area associated with the truss element as part of the section definition. When truss elements are used in large-displacement analysis, the updated cross-sectional area is calculated by assuming that the truss is made of an incompressible material, regardless of the actual material definition. The input material parameters of RC panel for compression and tension for CDP model are derived based on the Hsu and Hsu stress strain model as shown in Table 2 and Table 3. Poisson's ratio and Modulus of elasticity are chosen to be 0.2 and 31623 MPa. Table 4 and Table 5 show the material properties of steel reinforcement. The meshed model of RC panel and the projectile is shown in Fig. 5.

4.2. Plain concrete panel penetrated with ogive-nosed projectile

The impact behavior of reinforced concrete panel investigated experimentally by Wu et al. [42] is modeled numerically in the present part. It consists of RC panel of dimensions 675 mm × 675 mm × 200 mm penetrated with an ogive-nosed

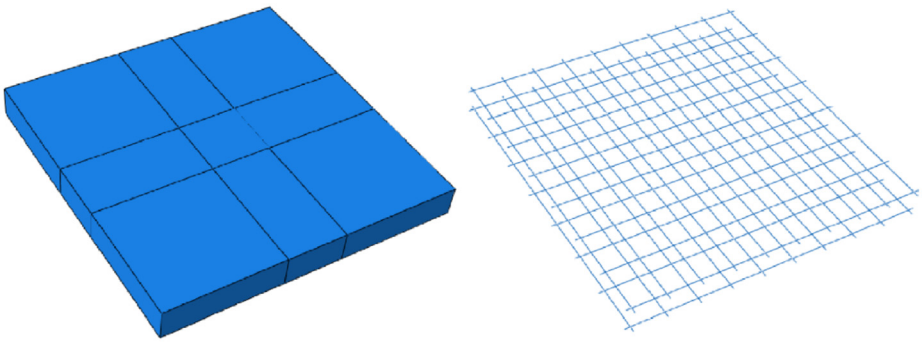

Fig. 4. (a) Concrete slab and (b) steel reinforcement in RC panel.

Table 2
Material parameters of concrete in compression for CDP model.

Inelastic Strain	Yield Stress	Compressive Damage
0.0000×10^{0}	15.4952	0.0000
7.3108×10^{-5}	28.9947	0.0055
2.4923×10^{-4}	39.2367	0.0189
5.5450×10^{-4}	45.3945	0.0419
9.7268×10^{-4}	47.9819	0.0736
1.4718×10^{-3}	48.0112	0.1113
2.0204×10^{-3}	46.4718	0.1528
2.5952×10^{-3}	44.1072	0.1963
3.1808×10^{-3}	41.4001	0.2406
3.7683×10^{-3}	38.6347	0.2850
4.3527×10^{-3}	35.9644	0.3293
4.9318×10^{-3}	33.4634	0.3731
5.5046×10^{-3}	31.1606	0.4164
6.0710×10^{-3}	29.0603	0.4592
6.6313×10^{-3}	27.1537	0.5016
7.1859×10^{-3}	25.4266	0.5436
7.7354×10^{-3}	23.8624	0.5851
8.2802×10^{-3}	22.4445	0.6263
8.8209×10^{-3}	21.1573	0.6672
9.3580×10^{-3}	19.9863	0.7079
9.8917×10^{-3}	18.9186	0.7482
1.0423×10^{-2}	17.9429	0.7884
1.0951×10^{-2}	17.0490	0.8284

Table 3
Material parameters of concrete in tension for CDP model.

Tensile Stress	Cracking Strain	Tensile Damage
X	0	0
0	0.01	0.9

X is the tensile strength of concrete in N/mm^2.

Table 4
General and Elastic material properties of Steel.

Grade (Yield Strength in N·mm^{-2})	Fe-250
Density/(kg·m^{-3})	7850
Young's Modulus/(N·mm^{-2})	200000
Poisson's ratio	0.3

Table 5
Plastic Material Properties of Steel reinforcement.

Yield Stress/(N·mm^{-2})	Plastic Strain
332	0
352	0.0001
373	0.0003
394	0.001
435	0.002
435	0.003
440	0.005
435	0.01
400	0.03
370	0.06

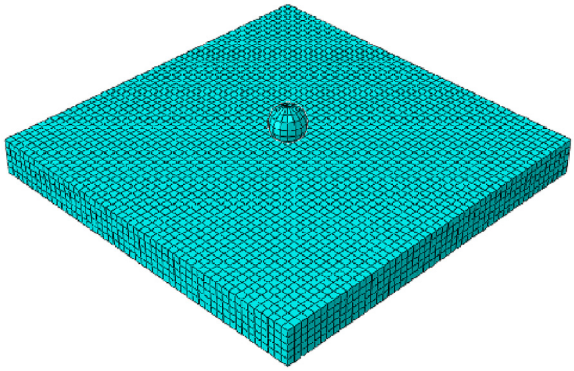

Fig. 5. Meshed model of RC panel and Projectile.

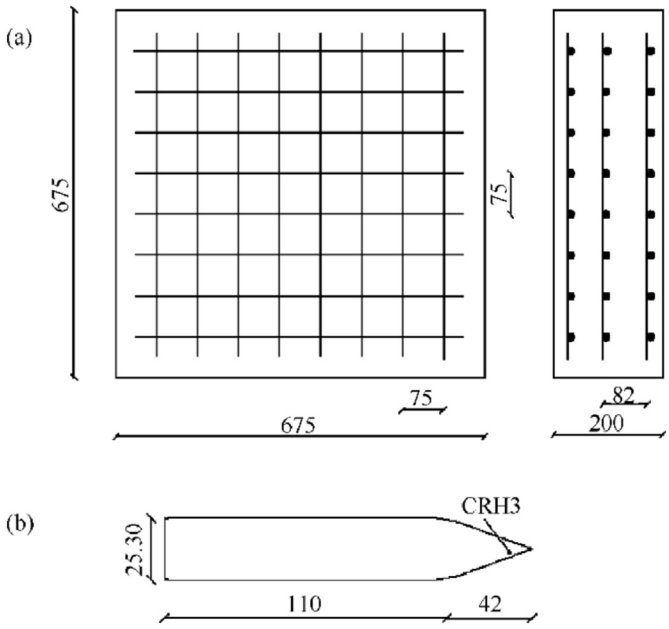

Fig. 6. (a) RC panel and (b) projectile geometries (dimensions in mm).

Table 6
Material parameters of the concrete material [48].

ρ/(kg·m^{-3})	G /GPa	A	B	n
2440	14.86	0.79	1.6	0
C	m	$\dot{\varepsilon}_0$	S_{max}	T/GPa
0.007	0.61	1	7	0.00354
$\bar{\varepsilon}^{pl}_{f,min}$	$\bar{\varepsilon}^{pl}_{f,max}$	D_1	D_2	K_1 /GPa
0.001	1	0.04	1	85
K_2 /GPa	K_3 /GPa	K_3 /GPa	P_{HEL} /MPa	
−171	208	80	48	

rigid steel projectile under 540 m/s to 745 m/s of velocities. Fig. 6 illustrates the geometry details of the RC panel and steel projectile. Three orthogonal layers of steel with diameter of 6 mm are embedded internally in concrete with concrete cover of 15 mm in-depth. The ogive-nosed steel projectile has length of 152 mm, diameter of 25.30 mm and caliber-radius-head (CRH) ratio of 3.00. The RC panel is modeled using the JH-2 and CDP models using the commercial package Abaqus/Explicit. The JH-2 model parameters are obtained from [48] (Table 6). The input material and CDP parameters of RC panel for compression and tension for CDP are the same shown above in Table 2 to Table 5.

Analytical rigid element with a mass assigned at a reference point and initial velocity of 540 m/s is adapted in the modeling of the projectile. General contact between the projectile and the concrete surface panel is used. It was considered by Wu et al. [42] that the projectile should always be impacted between the steel reinforcement. Consequently, the effect of steel reinforcement on the impact resistance is neglected in the present work. [45] showed that the effect of steel reinforcement on concrete resistance under

impact loads is negligible since the diameter is much smaller than the grid size of the steel reinforcement. Therefore, plain concrete is considered in the present work in the aim to simplify the numerical modeling. In order to reduce the computational analysis time, only a half of the concrete sample and the projectile is considered as shown in Fig. 5. Three-dimensional eight node reduced integration (C3D8R) element was adopted with 5 mm × 5 mm × 5 mm of mesh at the impact location, and 20 mm × 20 mm × 20 mm of mesh at the outer region (Fig. 7).

5. Results and discussion

5.1. RC concrete penetrated with spherical projectile

The analysis is performed for varying low-impact velocities and the behavior of the slab in terms of its failure stress is shown in Fig. 8.

From Fig. 8, it was observed that the Von Mises stress increases slightly as the velocity of impact object increases. There is a decrease in stress from velocity 6 m/s to 8 m/s, however, the difference is small enough to neglect and therefore it is seen that Von Mises stress has a gradual increase as the velocity increases. The deviation from 6 m/s-8 m/s is increased which is due to the increase in size of the impact object.

Residual velocity of the impact object of size 150 mm diameter for varying velocities is plotted in a graphical form as shown in Fig. 9.

Scabbing was observed when the slab is subjected to high strain rate loading as shown in Fig. 10. Scabbing of concrete is caused due to the interference between the tension wave and the compression wave (reflected from the immediate next surface).

5.2. Plain concrete panel penetrated with ogive-nosed projectile

The impact behavior of RC panel is investigated numerically using finite element tool ABAQUS/Explicit. JH-2 model and CDP model are adopted in the study to compare the behavior of RC panel using both the models. The following observations are made comparing both the models as shown in Table 7.

Contact pressure and time taken to penetrate the object using both models are comparable to each other as shown in Table 7. Damage of concrete in compression was shown in Fig. 11. From this figure, it can be observed that the damage has initiated and propagated very quickly using CDP model as the failure criteria considers damage in compression to full extent. Compared to JH-2 model the concrete panel had fractured severely using CDP model indicating the fact that the cracking was distributed along the length of the panel from the point of contact of the projectile. Similar behavior was observed in case of Von Mises stresses and the equivalent plastic strain of the concrete panel using CDP model as shown in Fig. 12 and Fig. 13.

From Fig. 13, it can be seen that the concrete cracking was perpendicular to the length of the panel and it increases with the increase in the velocity of the projectile from the point of contact.

Fig. 14 shows the internal energy of concrete and kinetic energy of projectile analyzed using JH-2 and CDP models respectively. In both the cases the kinetic energy of projectile decreased from the point of contact of concrete panel. The rate of decrement was almost same for both the models till 400 μs and had increased for

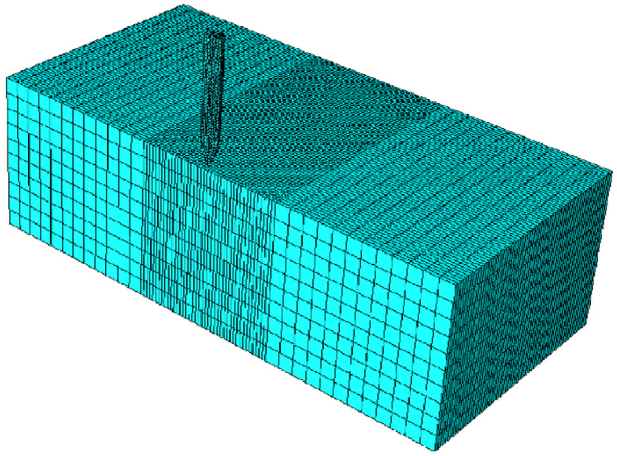

Fig. 7. Finite element discretization the concrete panel and steel projectile.

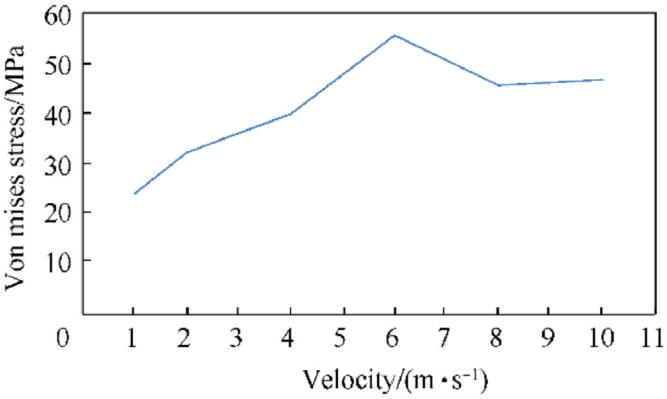

Fig. 8. Von Mises stress for 150 mm impact object with varying velocities.

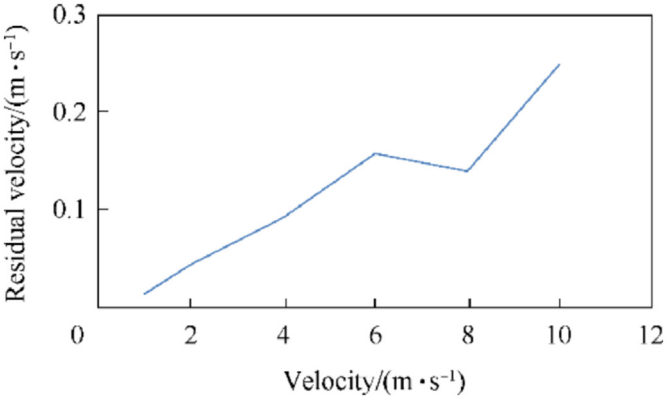

Fig. 9. Velocity vs residual velocity of 150 mm diameter projectile.

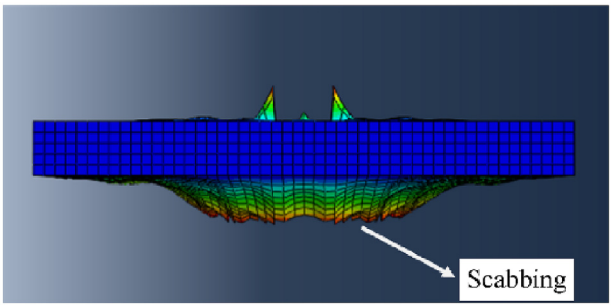

Fig. 10. Scabbing in slab subjected to impact loading by 150 mm object with 2 m/s velocity.

Table 7
Comparison between JH-2 and CDP models for impact analysis of RC panel.

Parameter	JH-2 Model	CDP Model	% Difference
Contact pressure/(N·mm^{-2})	0-(1.35 × 10^7)	0-(1.15 × 10^7)	13%
Time taken to penetrate object/s	0.001	0.000954	4.6%

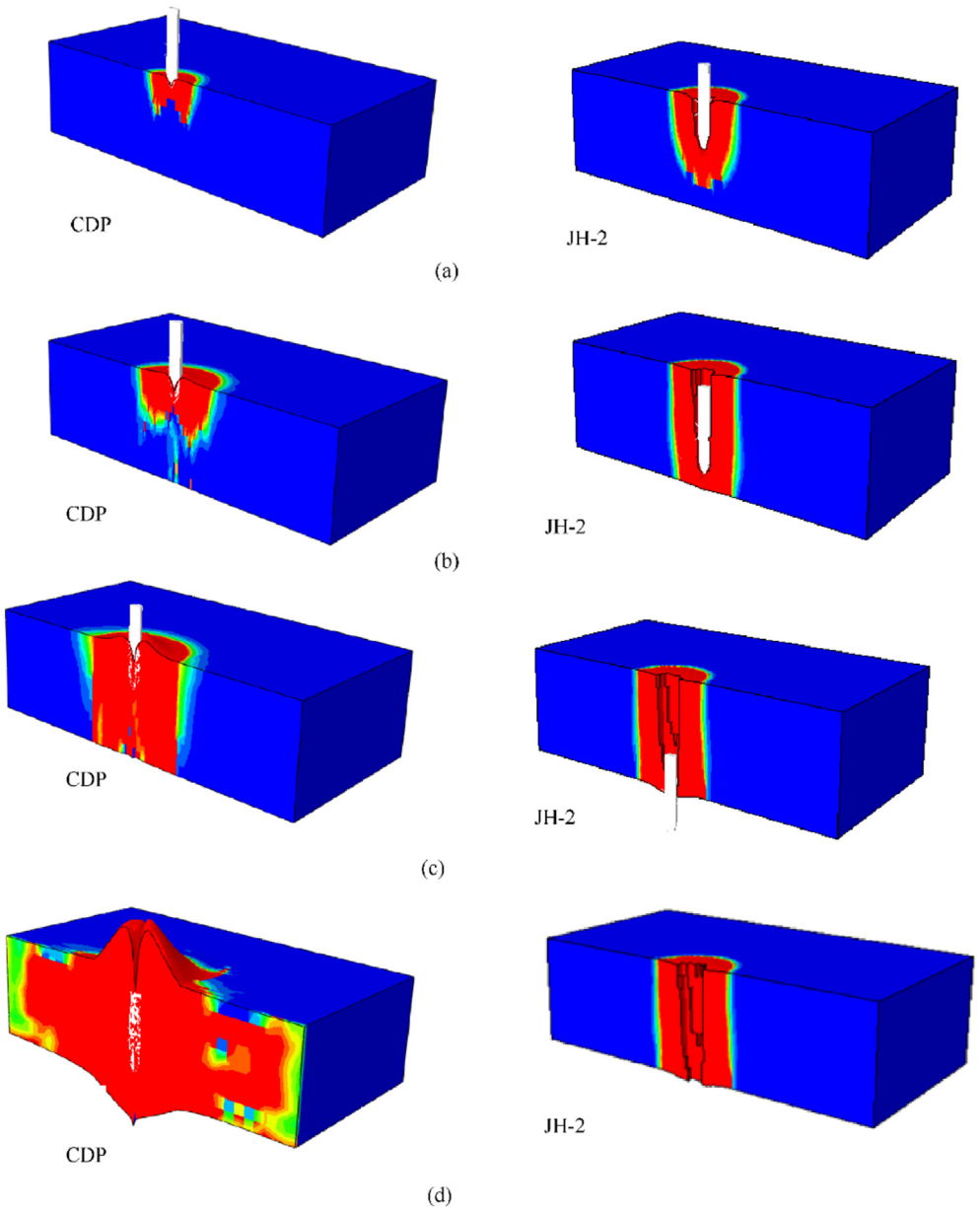

Fig. 11. Damage contour in concrete: (a) $t = 0.0002$ **s**, (b) $t = 0.0004$**s**, (c) $t = 0.0007$ **s**.

CDP model beyond that as the brittleness of the concrete model increased from the point of contact of the projectile. The case of internal energy of concrete is less in the case of CDP model compared to JH-2 model.

6. Conclusions

Numerical analysis of impact behavior of reinforced and plain concrete panels subjected to low and high velocities was conducted in this work. The first part of the present paper assessed the low velocity impact of an RC panel. The spherical steel projectile was used in this part. The results revealed an increase in Von Mises stress as the velocity of the impact object increases with a minor exception from velocity 6 m/s to 8 m/s. Von Mises stress shows gradual increase as the diameter of the impact object increases. There was a slight increase in the residual velocity of the impact object with the increasing impact velocity. Scabbing and mesh element irregularity increases as the force of impact increases because more elements are ejected from the bottom of the slab.

The study was further extended for a comparative analysis of

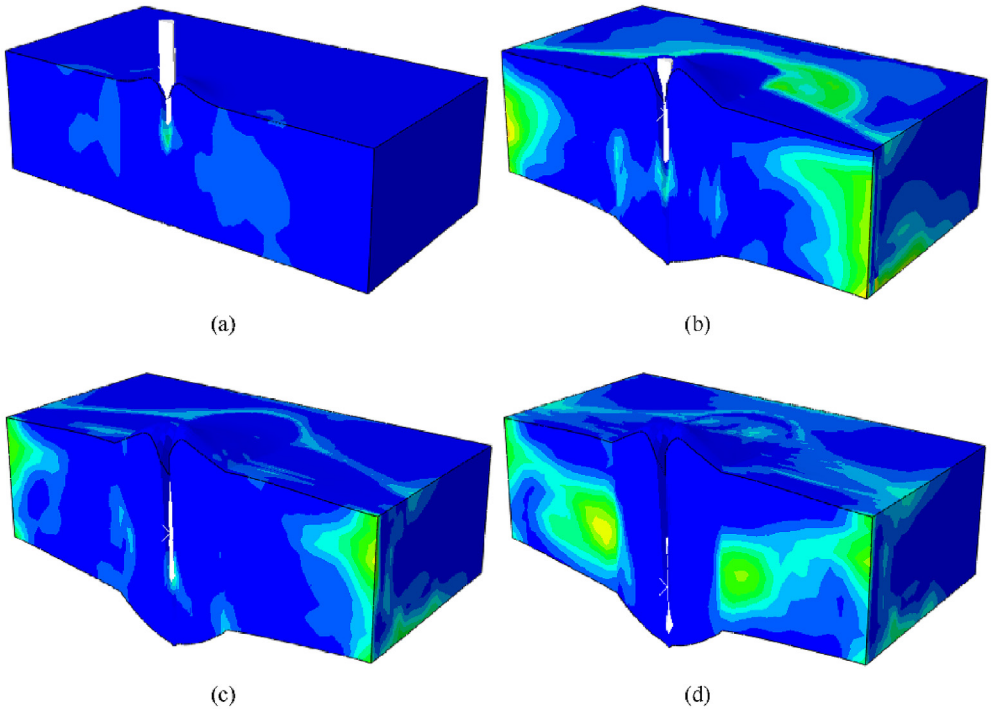

Fig. 12. Von Mises stress for concrete panel: (a) $t = 0.0002$ s, (b) $t = 0.0004$ s, (c) $t = 0.0007$ s, (d) $t = 0.001$ s.

CDP and JH-2 damage models. The behavior of plain concrete was considered as the impact resistance of steel reinforcement is neglected. The steel ogive-nosed projectile used was simulated as a rigid body with a mass of 0.386 kg assigned at a reference point. Damage was evaluated using JH-2 model and a comparative behavior of damage of concrete panel was done between CDP and JH-2. Concrete panel fractured severely in the case of CDP model much before the JH-2 model. Comparison was also done for internal and kinetic energies of concrete panel and the steel projectile, respectively. As soon as the steel projectile started penetrating into the concrete panel the kinetic energy of the projectile started decreasing. The final kinetic energy of the projectile was more

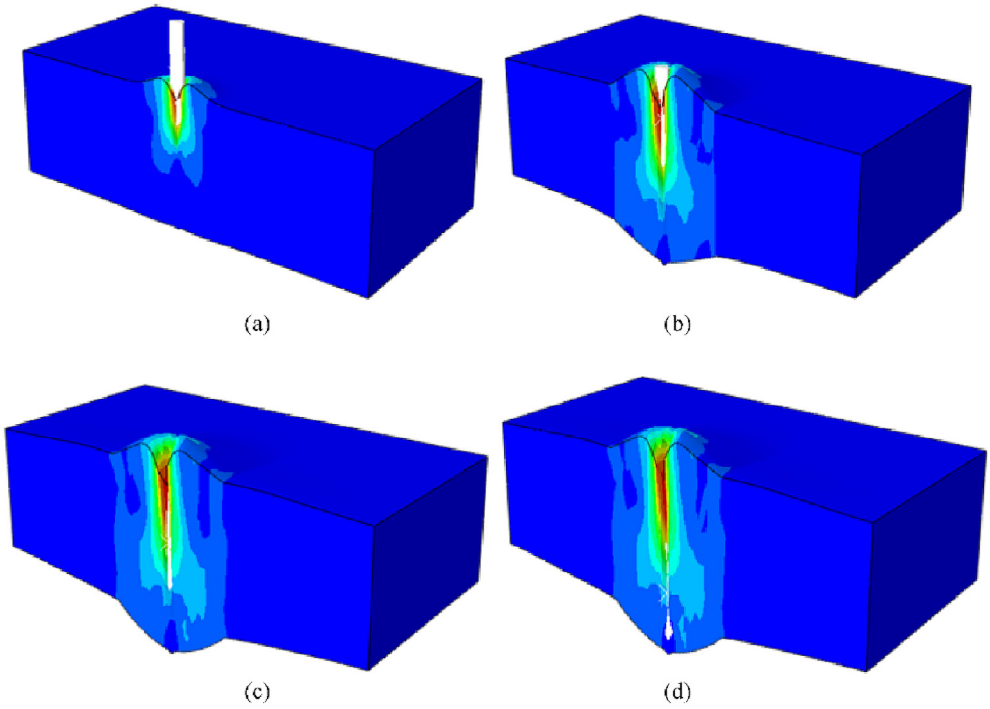

Fig. 13. Equivalent Plastic strain of concrete panel: (a) $t = 0.0002$ s, (b) $t = 0.0004$ s, (c) $t = 0.0007$ s, (d) $t = 0.001$ s.

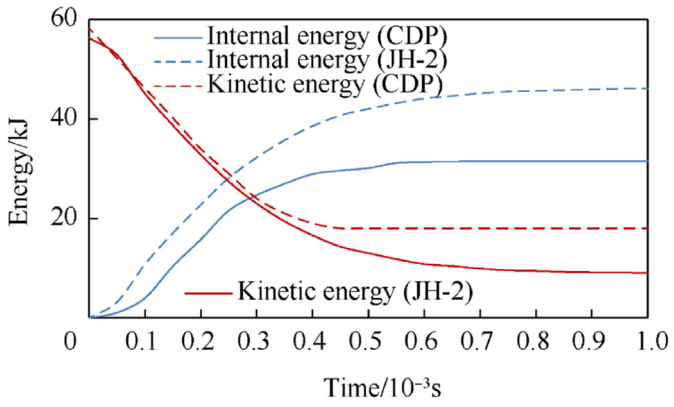

Fig. 14. Internal Energy of concrete and Kinetic Energy of Projectile.

using CDP model. The internal energy of concrete using CDP model was less as the concrete panel fractured rapidly as soon as the projectile started penetrating onto the concrete panel. It can also be understood that both JH-2 and CDP models can be used for assessing the impact behavior of plain concrete model subjected to high-velocity impact loading and CDP model can be utilized for reinforced concrete panels subjected to low-velocity impact. The present work can further be extended to mesh independent JH-2 and CDP models for a better accuracy of the representing the experimental behavior of concrete panels.

Dedicate

The first author dedicates this work to the memory of his co-worker Dr. Kheira Ouzaa.

Declaration of competing interest

The authors declare that they have no known competing financial interests or personal relationships that could have appeared to influence the work reported in this paper.

Acknowledgements

The second author would like to acknowledge computing lab facilities of Vignana Bharathi Institute of Technology sponsored by DST-FIST. Second and third authors would like to acknowledge the computational facilities provided by Simulia ABAQUS CAE at BITS Pilani-Hyderabad Campus.

References

[1] Plotzitza A, Rabczuk T, Eibl J. Techniques for numerical simulations of concrete slabs for demolishing by blasting. J Eng Mech 2007;133(5):523–33.
[2] Rabczuk T, Akkermann J, Eibl J. A numerical model for reinforced concrete structures. Int J Solid Struct 2005;42(5–6):1327–54.
[3] Rabczuk T, Belytschko T. Application of particle methods to static fracture of reinforced concrete structures. Int J Fract 2006;137(1–4):19–49.
[4] Rabczuk T, Zi G, Bordas S, Nguyen-Xuan H. A geometrically non-linear three-dimensional cohesive crack method for reinforced concrete structures. Eng Fract Mech 2008;75(16):4740–58.
[5] Rabczuk T, Belytschko T. Cracking particles: a simplified meshfree method for arbitrary evolving cracks. Int J Numer Methods Eng 2004;61(13):2316–43.
[6] Rabczuk T, Belytschko T. A three dimensional large deformation meshfree method for arbitrary evolving cracks. Comput Methods Appl Mech Eng 2007;196(29–30):2777–99.
[7] Rabczuk T, Samaniego E, Belytschko T. Simplified model for predicting impulsive loads on submerged structures to account for fluid-structure interaction. Int J Impact Eng 2007;34(2):163–77.
[8] Rabczuk T, Zi G, Bordas S, Nguyen-Xuan H. A simple and robust three-dimensional cracking-particle method without enrichment. Comput Methods Appl Mech Eng 2010;199(37–40):2437–55.
[9] Rabczuk T, Song JH. Preface to SI: experimental testing and computational modeling of dynamic fracture. Int J Impact Eng 2016;87:2.
[10] Kalameh HA, Karamali A, Anitescu C, Rabczuk T. High velocity impact of metal sphere on thin metallic plate using smooth particle hydrodynamics (SPH) method. Front Struct Civ Eng 2012;6(2):101–10.
[11] Amani J, Oterkus E, Areias P, Zi G, Nguyen-Thoi T, Rabczuk T. A non-ordinary state-based peridynamics formulation for thermoplastic fracture. Int J Impact Eng 2016;87:83–94.
[12] Gui YL, Bui HH, Kodikara J, Zhang QB, Zhao J, Rabczuk T. Modelling the dynamic failure of brittle rocks using a hybrid continuum-discrete element method with a mixed-mode cohesive fracture model. Int J Impact Eng 2016;87:146–55.
[13] Areias P, Msekh MA, Rabczuk T. Damage and fracture algorithm using the screened Poisson equation and local remeshing. Eng Fract Mech 2016;158:116–43. 2016.
[14] Diyaroglu C, Oterkus E, Madenci E, Rabczuk T, Siddiq A. Peridynamic modeling of composite laminates under explosive loading. Compos Struct 2016;144:14–23.
[15] Hu F, Wu H, Fang Q, Liu JC, Liang B, Kong XZ. Impact performance of explosively formed projectile (EFP) into concrete targets. Int J Impact Eng 2017;109:150–66.
[16] Reza Ghasemi M, Shishegaran A. Role of slanted reinforcement on bending capacity SS beams. Vibroengineering PROCEDIA 2017;11:195–9.
[17] Rodriguez-Millan M, Garcia-Gonzalez D, Rusinek A, Abed F, Arias A. Perforation mechanics of 2024 aluminium protective plates subjected to impact by different nose shapes of projectiles. Thin-Walled Struct 2018;123:1–10.
[18] Oucif C, Mauludin LM. Numerical modeling of high velocity impact applied to reinforced concrete panel. Undergr Space 2019;4(1):1–9.
[19] Oucif C, Mauludin LM, Abed Farid. Ballistic behavior of plain and reinforced concrete slabs under high velocity impact. Front Struct Civ Eng 2019:1–24. https://doi.org/10.1007/s11709-019-0588-5.
[20] Shishegaran A, Khalili MR, Karami B, Rabczuk T, Shishegaran A. Computational predictions for estimating the maximum deflection of reinforced concrete panels subjected to the blast load. Int J Impact Eng 2020:103527.
[21] Voyiadjis GZ, Abed FH. Transient localizations in metals using microstructure-based yield surfaces. Model Simulat Mater Sci Eng 2006;15(1):S83.
[22] Abed Farid H, AL-Tamimi, Adil K, Himairee, Reem M, et al. Characterization and modeling of ductile damage in structural steel at low and intermediate strain rates. J Eng Mech 2012;138(9):1186–94.
[23] Darras BM, Abed FH, Pervaiz S, Abdu-Latif A. Analysis of damage in 5083 aluminum alloy deformed at different strainrates. Mater Sci Eng 2013;568:143–9.
[24] Abed FH, Saffarini MH, Abdul-Latif A, Voyiadjis GZ. Flow stress and damage behavior of C45 Steel over a range of temperatures and loading rates. J Eng Mater Technol 2017;139(2):021012.
[25] Oucif C, Voyiadjis GZ, Rabczuk T. Modeling of damage-healing and nonlinear self-healing concrete behavior: application to coupled and uncoupled self-healing mechanisms. Theor Appl Fract Mech 2018;96:216–30.
[26] Levi-Hevroni D, Kochavi E, Kofman B, Gruntman S, Sadot O. Experimental and numerical investigation on the dynamic increase factor of tensile strength in concrete. Int J Impact Eng 2018;114:93–104.
[27] Borvik T, Langseth M, Hopperstad OS, Polanco-Loria MA. Ballistic perforation resistance of high performance concrete slabs with different unconfined compressive strengths. WIT Trans Built Environ 2002;59.
[28] Aslani F, Nejadi S. Mechanical properties of conventional and self-compacting concrete: an analytical study. Construct Build Mater 2012;36:330–47.
[29] Grégoire D, Rojas-Solano LB, Pijaudier-Cabot G. Failure and size effect for notched and unnotched concrete beams. Int J Numer Anal Methods GeoMech 2013;37(10):1434–52.
[30] Lopez-Almansa F, Alfarah B, Oller S. Numerical simulation of RC frame testing with damaged plasticity model. Comparison with simplified models. In: Second European conference on earthquake engineering and seismology. Turkey: Istanbul; 2014.
[31] Temsah Y, Jahami A, Khatib J, Sonebi M. Numerical analysis of a reinforced concrete beam under blast loading. In: MATEC Web of Conferences, 149; 2018, 02063.
[32] Othman H, Marzouk H. Applicability of damage plasticity constitutive model for ultra-high performance fibre-reinforced concrete under impact loads. Int J Impact Eng 2018;114:20–31.
[33] Liu J, Wu C, Su Y, Li J, Shao R, Chen G, Liu Z. Experimental and numerical studies of ultra-high performance concrete targets against high-velocity projectile impacts. Eng Struct 2018;173:166–79.
[34] Drathi R, Das AJM, Rangarajan A. Meshfree simulation of concrete structures and impact loading. Int J Impact Eng 2016;91:194–9.
[35] Kalyana Rama JS, Chauhan DR, Sivakumar MVN, Vasan A, Murthy AR. Fracture properties of concrete using damaged plasticity model Aparametric study. Struct Eng Mech 2017;64(1):59–69.
[36] Kota SK, Rama JS, Murthy AR. Strengthening RC frames subjected to lateral load with Ultra High-Performance fiber reinforced concrete using damage plasticity model. Earthquakes Strut 2019;17(2):221–32.
[37] Jankowiak T, Lodygowski T. Identification of parameters of concrete damage plasticity constitutive model. Found Civil Environ Eng 2005;6(1):53–69.
[38] Kmiecik P, Kamiński M. Modelling of reinforced concrete structures and composite structures with concrete strength degradation taken into consideration. Arc Civil Mech Eng 2011;11(3):623–36.

[39] Lubliner J, Oliver J, Oller S, Oñate E. A plastic-damage model for concrete. Int J Solid Struct 1989;25(3):299–326.
[40] Lee J, Fenves GL. Plastic-damage model for cyclic loading of concrete structures. J Eng Mech 1998;124(8):892–900.
[41] Johnson GR, Holmquist TJ. A computational constitutive model for brittle materials subjected to large strains, high strain rates and high pressures. Shock wave High-Strain-Rate Phen. Mater 1992:1075–81.
[42] Wu H, Fang Q, Peng Y, Gong ZM, Kong XZ. Hard projectile perforation on the monolithic and segmented RC panels with a rear steel liner. Int J Impact Eng 2015;76:232–50.
[43] Documentation, Abaqus, and User Manual. Dassault systemes. 2010. Version 6.10.
[45] Huang F, Wu H, Jin Q, Zhang Q. A numerical simulation on the perforation of reinforced concrete targets. Int J Impact Eng 2002;32(1–4):173–87.
[47] Hofstetter BVG. Review and enhancement of 3D concrete models for large-scale numerical simulations of concrete structures. Int J Numer Anal Methods GeoMech 2013;37(3):221–46.
[48] Johnson GR, Holmquist TJ. An improved computational constitutive model for brittle materials. 1994. In: AIP Conference Proceedings, 309; 1994, July. p. 981–4. 1.